Molecular and Functional Mapping of the Piebald Deletion Complex on Mouse Chromosome 14

Jeffrey J. Roix,*,[1] Aaron Hagge-Greenberg,*,[1] Dennis M. Bissonnette,*,[2] Sandra Rodick,* Liane B. Russell† and Timothy P. O'Brien*

**The Jackson Laboratory, Bar Harbor, Maine 04609 and †Biology Division, Oak Ridge National Laboratory, Oak Ridge, Tennessee 37831*

Manuscript received August 25, 2000
Accepted for publication November 13, 2000

ABSTRACT

The piebald deletion complex is a set of overlapping chromosomal deficiencies surrounding the endothelin receptor B locus collected during the Oak Ridge specific-locus-test mutagenesis screen. These chromosomal deletions represent an important resource for genetic studies to dissect the functional content of a genomic region, and several developmental defects have been associated with mice homozygous for distinct piebald deletion alleles. We have used molecular markers to order the breakpoints for 20 deletion alleles that span a 15.7–18-cM region of distal mouse chromosome 14. Large deletions covering as much as 11 cM have been identified that will be useful for regionally directed mutagenesis screens to reveal recessive mutations that disrupt development. Deletions identified as having breakpoints positioned within previously described critical regions have been used in complementation studies to further define the functional intervals associated with the developmental defects. This has focused our efforts to isolate genes required for newborn respiration and survival, skeletal patterning and morphogenesis, and central nervous system development.

THE mouse piebald deletion complex on distal chromosome 14 was assembled as part of the specific-locus-test (SLT) mutagenesis screen conducted over the past five decades at the Oak Ridge National Laboratory (Russell 1951; Davis and Justice 1998). In the SLT experiments, genetic lesions including point mutations, chromosomal rearrangements, and intra- and multilocus deletions were recovered at seven different loci that when mutated yield viable and readily visible recessive phenotypes. In the SLT screen, mutagenized (101 × C3H) F_1 males were mated with Tester-stock females harboring recessive mutations at the seven specific loci: non-agouti (*a*), brown [*b*, tyrosinase-related protein 1 (*Tyrp1*)], albino [*c*, tyrosinase (*Tyr*)], pink-eyed dilution (*p*), dilute [*d*, myosinVa (*Myo5a*)], short-ear [*se*, bone morphogenetic protein 5 (*Bmp5*)], and piebald [*s*, endothelin receptor B (*Ednrb*)]. Designed to assess the genetic risks associated with radiation and chemical mutagens, the SLT and the resulting deletion complexes have also been used extensively for functional genomic studies (reviewed in Rinchik and Russell 1990). For example, complementation and phenotypic analysis using the albino deletion stocks coupled with a high-efficiency region-specific mutagenesis screen using the point mutagen *N*-ethyl-*N*-nitrosourea (ENU) has allowed the identification and characterization of genes essential for development within a 6- to 11-cM interval surrounding the *Tyr* locus on chromosome 7 (Russell *et al.* 1982; Niswander *et al.* 1989; Holdener-Kenny *et al.* 1992; Schumacher *et al.* 1996; Rinchick and Carpenter 1999).

The piebald mutation disrupts *Ednrb* gene function, which is required for the development of neural crest-derived melanocytes and enteric ganglia (Hosoda *et al.* 1994; Pavan and Tilghman 1994; Shin *et al.* 1999). Mice homozygous for piebald ($Ednrb^{s}$), a partial loss-of-function spontaneous allele, are viable and exhibit white spotting covering ~20% of their coat. Another spontaneous allele, piebald lethal ($Ednrb^{s\text{-}l}$), is a deletion at the piebald locus. $Ednrb^{s\text{-}l}/Ednrb^{s\text{-}l}$ mice as well as mice homozygous for a targeted disruption of *Ednrb* are almost completely white and exhibit megacolon resulting in lethality as juveniles or young adults, typically 2–8 wk after birth (Lane 1966; Hosoda *et al.* 1994).

The homozygous phenotype of mice harboring SLT-induced mutations at the piebald locus has allowed these alleles to be grouped into two classes: those that present juvenile lethality and those that are peri- or prenatally lethal. Molecular analysis has demonstrated that alleles of the first class are often not deletions, but rather mutations affecting expression or protein structure that result in the severe reduction or loss of *Ednrb* gene function (Shin *et al.* 1997). The alleles in the second class are chromosomal deletions believed to remove genes in addition to *Ednrb* essential for survival

Corresponding author: Timothy P. O'Brien, The Jackson Laboratory, 600 Main St., Bar Harbor, ME 04609. E-mail: tpo@jax.org

[1] These authors contributed equally to this work.

[2] *Present address:* Department of Neurobiology and Behavior, Cornell University, Ithaca, NY 14853.

until or shortly after birth (Metallinos *et al.* 1994; O'Brien *et al.* 1996).

In previous studies we have characterized several developmental defects associated with three of the piebald deletion alleles. Embryos homozygous for the *Ednrb$^{s\text{-}1Acrg}$* deletion (hereafter, SLT-induced deletions are abbreviated using allele names, *i.e.*, *Ednrb$^{s\text{-}1Acrg}$* = *1Acrg*) die at midgestation and exhibit perturbations in mesoderm development and left-right morphogenesis (Welsh and O'Brien 2000). Mice homozygous for the *15DttMb* or *36Pub* deletions experience respiratory distress and die shortly following birth (O'Brien *et al.* 1996). In addition, these mice display central nervous system (CNS) abnormalities and alterations in skeletal morphogenesis and patterning. Molecular and genetic analysis has localized the phenotypes to defined functional intervals within each of these deletions. In an effort to further the piebald deletion complex as a resource for region-specific functional analysis we have used molecular markers to map the distribution of the breakpoints for 20 deletions, including 12 previously uncharacterized SLT-induced alleles, that span a 15.7- to 18-cM segment of distal chromosome 14. Distinct sets of deletions identified as having critically positioned breakpoints have been used in complementation studies to genetically dissect and refine the previously identified functional intervals, with efforts focused on isolating genes important for newborn survival, CNS, and skeletal development.

MATERIALS AND METHODS

Mice: The piebald deletion stock mice were generated at the Oak Ridge National Laboratory by chemical or radiation mutagenesis of (101/Rl × C3H/Rl) F_1 males followed by mating with Tester-stock females homozygous for the seven SLT mutations including the *Ednrb^s* allele. The mice used in this study were obtained as heterozygous deletion stocks following the test cross between *Ednrb^s* and the parental deletion stock, which had been maintained by crossing with (101/Rl × C3H/Rl) F_1 mice. The piebald deletion stock mice were mated with CAST/Ei mice to introduce polymorphisms used in the molecular mapping studies. CAST/Ei heterozygous deletion carriers were identified in a PCR reaction using *D14Mit8*, which resolves the *Ednrb^s*, CAST/Ei, and the deletion carrying C3H or 101 chromosomes. The piebald deletion stock mice used in the complementation and phenotype analyses were obtained by Caesarian rederivation following matings with C57BL/6J mice. C57BL/6J heterozygous deletion mice were initially identified in a PCR reaction using *D14Mit265*, which distinguishes the *Ednrb^s*, C57BL/6J, and the C3H or 101 chromosomes. The piebald deletion colonies were subsequently maintained and expanded by mating with C57BL/6J mice. For expansion, deletion heterozygous mice were identified in PCR genotyping assays using markers *D14Mit225* or *D14Mit265* (proximal) and *D14Mit185* (distal) that flank the deletion breakpoints and distinguish the C57BL/6J and deletion-carrying C3H or 101 chromosomes. The results of the genotyping assays were confirmed by scoring for almost completely white offspring following test crosses between deletion heterozygous and SSL/Le *Ednrb^s/Ednrb$^{s\text{-}l}$* mice. At the time of this study the *4Pub, 4CHLc, 24Pub, 17Pub, 1XMLP, 1XMLPc, 9ThW, 48UThc, 13Pub, 31Pub, 1MLPf, 2MLPl, 29Pub, 1Pu, 27Pu,* and *52Pub* mice had been backcrossed with C57BL/6J for two generations. The *36Pub, 15DttMb,* and *1Acrg* mice had been backcrossed with C57BL/6J for six generations. The SSL/Le *Ednrb^s/Ednrb$^{s\text{-}l}$* mice were obtained from The Jackson Laboratory mutant resource as a F102 inbred stock. *Ednrb^s/Ednrb$^{s\text{-}l}$* intercross offspring were genotyped using *D14Mit8* as previously described (Metallinos *et al.* 1994).

Deletion homozygous and compound heterozygous mice were generated by intercross matings of the various deletion heterozygous mice. All of these mice were initially genotyped in a PCR reaction using *D14Mit265*. The *D14Mit265* marker is present on at least one of the chromosomes carried by all of the deletion allele combination mice produced in these crosses. Therefore, amplification of a unique C3H/101 product identified the deletion homozygous or compound heterozygous mice. The initial genotyping was verified by confirming the absence of the *Ednrb* locus from the commonly held deletion region using a PCR assay as previously described (O'Brien *et al.* 1996).

Molecular analysis of the induced *Ednrb^s* alleles: The *D14Mit* $(CA)_n$ repeat markers (MapPair primers; Research Genetics, Huntsville, AL) used for defining the deletion limits were selected on the basis of the presence of a polymorphism between C3H/101 and CAST/Ei or C57BL/6J chromosomes and their representation of a unique position on the Whitehead Institute/MIT Center for Genome Research (WI/MIT CGR) or the Mouse Genome Database/Chromosome Committee Report (MGD/CCR) genetic map. All of the markers were used in PCR reactions to assay a panel of DNAs that included the parental controls CAST/Ei or C57BL/6J and *Ednrb$^{s\text{-}Del}$/Ednrb^s*, a littermate control *Ednrb^s*/CAST/Ei (or C57BL/6J), and a deletion carrier *Ednrb$^{s\text{-}Del}$*/CAST/Ei (or C57BL/6J). The size polymorphisms in base pairs for each *D14Mit* product used to identify the CAST/Ei, C57BL/6J, *Ednrb^s (s)* and *Ednrb$^{s\text{-}Del}$* (C3H or 101) alleles are provided in Table 1.

The STS markers used in these studies were generated from the sequences of the ends of bacterial artificial chromosomes (BACs) that have been assembled into contigs following PCR screening of the CJ7 129SV ES cell-derived BAC library (Research Genetics) using various markers previously mapped to the region (Metallinos 1994). The *D14Jax* STS product sizes and forward and reverse primer pair sequences are provided in Table 2. All of the *D14Jax* STS and the *D14Mit: 8, 93, 94, 205, 166, 167, 197, 165, 42* and *118* markers were assayed in PCR reactions using deletion homozygous or compound heterozygous DNAs produced from the various complementation crosses. Therefore, content could be determined on the basis of the presence or absence of the marker and a polymorphism was not required. Genomic DNA from tail tip, embryonic liver, or extraembryonic yolk sac tissues was prepared as previously described (Metallinos *et al.* 1994).

PCR reactions were carried out in a 15-μl reaction containing 0.2 mm dNTP (Promega, Madison, WI), 1 mm $MgCl_2$ (Perkin-Elmer, Boston, MA), 1 μm forward and reverse primer, 0.75 units *Taq* DNA polymerase (Perkin-Elmer), 200 ng DNA, and 1× *Taq* polymerase buffer (10 mm Tris-HCl pH 8.3 at 25°, 50 mm KCl; Perkin-Elmer). PCR reactions for all of the markers except *D14Mit8* and *D14Mit185* were performed using a PTC-200 Thermocycler (MJ Research, Waltham, MA) as follows: incubation for 3 min at 94°, 12 cycles of denaturation at 94° for 20 sec, annealing at 64° shifting to 58° in 0.5° increments for 30 sec, and extension at 72° for 35 sec. This was followed by 25 cycles of denaturation at 94° for 20 sec, annealing at 58° for 30 sec, and extension at 72° for 35 sec. Reactions utilizing *D14Mit8* and *D14Mit185* were cycled as follows: incubation at 94° for 3 min, 35 cycles of denaturation at 94° for 30 sec, annealing at 55° for 58 sec, and extension at 72° for 1 min. PCR reaction products were resolved by polyacrylamide

TABLE 1

Allele sizes for *D14Mit* markers used in this study

Marker	CAST/Ei	C57BL/6J	*s*	C3H	101
D14Mit225	115	121	105	105	110
D14Mit116	145	143	143	141	138
D14Mit194	101	89	89	81	89
D14Mit125	146	158	115	122	159
D14Mit7	89	107	—	95	—
D14Mit219	130	119	199	109	120
D14Mit228	186	174	138	138	138
D14Mit264	122	106	—	100	100
D14Mit104	125	129	127	129	129
D14Mit265	178	148	150	178	178
D14Mit8	209	202	198	202	202
D14Mit145	123	141	—	141	—
D14Mit164	106	83	—	83	—
D14Mit38	152	144	144	144	144
D14Mit93	159	—	180	157	157
D14Mit94	79	107	109	107	195
D14Mit205	118	114	70	114	114
D14Mit166	151	144	—	128	124
D14Mit197	124	94	127	90	124
D14Mit167	142	135	143	135	—
D14Mit165	146	136	126	121	125
D14Mit42	176	152	146	152	152
D14Mit118	138	138	138	138	138
D14Mit95	137	129	180	129	129
D14Mit9	215	237	—	237	237
D14Mit185	144	142	142	128	130
D14Mit131	88	108	106	102	106
D14Mit266	156	148	148	176	147
D14Mit77	158	186	184	192	184
D14Mit267	90	116	117	116	118

Allele sizes are in base pairs. —, not determined.

gel electrophoresis using 12.5% acrylamide nondenaturing gels and products were visualized using ethidium bromide staining.

Histological and skeletal analysis: Embryos and fetuses collected for the histological and skeletal analyses were obtained from timed matings where noon of the day of detection of a vaginal plug was designated E0.5. Skeletal preparations and histology were performed as previously described (O'Brien *et al.* 1996).

RESULTS

Molecular mapping of the piebald deletion alleles: The simple sequence length polymorphism (SSLP) panel of *Mit* markers was used to construct a map of the piebald deletion complex (Dietrich *et al.* 1996; Figure 1). The breakpoints were resolved using DNA derived from each deletion mouse stock heterozygous for the mutagenized 101/Rl or C3H/Rl chromosome opposite either a CAST/Ei or C57BL/6J intact chromosome. This provided the opportunity to identify polymorphic SSLP *D14Mit* markers, allowing their presence or absence to be determined for each deletion chromosome. All 19 of the SLT-induced piebald alleles examined removed a subset of the molecular markers, confirming that each contained a deletion. *D14Mit116* and *D14Mit267* were present in all of the deletions examined and defined the proximal and distal ends of the complex, respectively. *D14Mit116* and *D14Mit267* delimit a region containing 74 SSLP markers mapping along a 17-cM segment of the MGD/CCR mouse chromosome 14 genetic map. We used a total of 29 of the SSLP markers representing 17 unique map positions to initially survey the distribution of deletion breakpoints across the region. In this way each deletion breakpoint was localized to an interval defined by the position of the SSLP markers on the genetic map. Deletions were identified that extended as far as 8 cM proximally and 10 cM distally from the piebald locus focal point, with *Ednrb*$^{s\text{-}l}$ being the smallest deletion at <1.0 cM and the largest deletions encompassing 10–12 cM (see Figure 1). The breakpoints were distributed across the 17-cM

TABLE 2

***D14Jax* STS markers used in this study**

Marker	Product	Forward	Reverse
D14Jax1	162	TAAGTCATGCCACATGCTGG	GGCCTTTTACCTTAGGCAGG
D14Jax3	387	AAGAGGACGTCTACCATGGC	TTGGAGCTGGAGTCATAGGC
D14Jax4	228	CATAGTGGCACACTCAATGC	ATTATGGTGGAAGCTGTGGC
D14Jax6	216	TTGGTGCTTCTCAGCACTTC	ACCTTTGATCCCAGCACTTG
D14Jax7	268	CACCTCTAACTGCATCTTAGG	GTGGGTGTGTACATTGGACA
D14Jax9	605	CCTGAACAGTCACATATCTTG	CCATCTTTCTATCTCTCTGTC
D14Jax10	360	CACCTCTTTAGTCACTCCTG	ATCTGTGCGTAGACTTCTTTG
D14Jax11	320	GACCTCACAGTTCATCCATG	TGAACTGCTTCACAGTGCTG
D14Jax12	260	TGAAAGAGAATAGCCTCAAGC	TATTCCAGTCTCTGAGCAGC
D14Jax13	240	TGGTCTGTGACACAGCTAAG	ACTGGAAATTAGGTCATGACC
D14Jax14	340	CGAGACGTGATGGTGTAAAG	TCTAACAGGACTGCACTGAG
D14Jax15	160	CGGGACTTAAATGCACTGACAGG	CCAGTCACAAGTAAGCACAAACCTC
D14Jax16	255	TTTTTTGCTGGAGGCAGGACTCC	TATAATTTGGGGGGAGGGGCAGAG
D14Jax21	240	CTCTGTGTCACAGGTAAGGTG	GAATCCGATGTCCGCACAGAC

Product sizes are in base pairs. Forward and reverse PCR primers were derived from BAC end sequences.

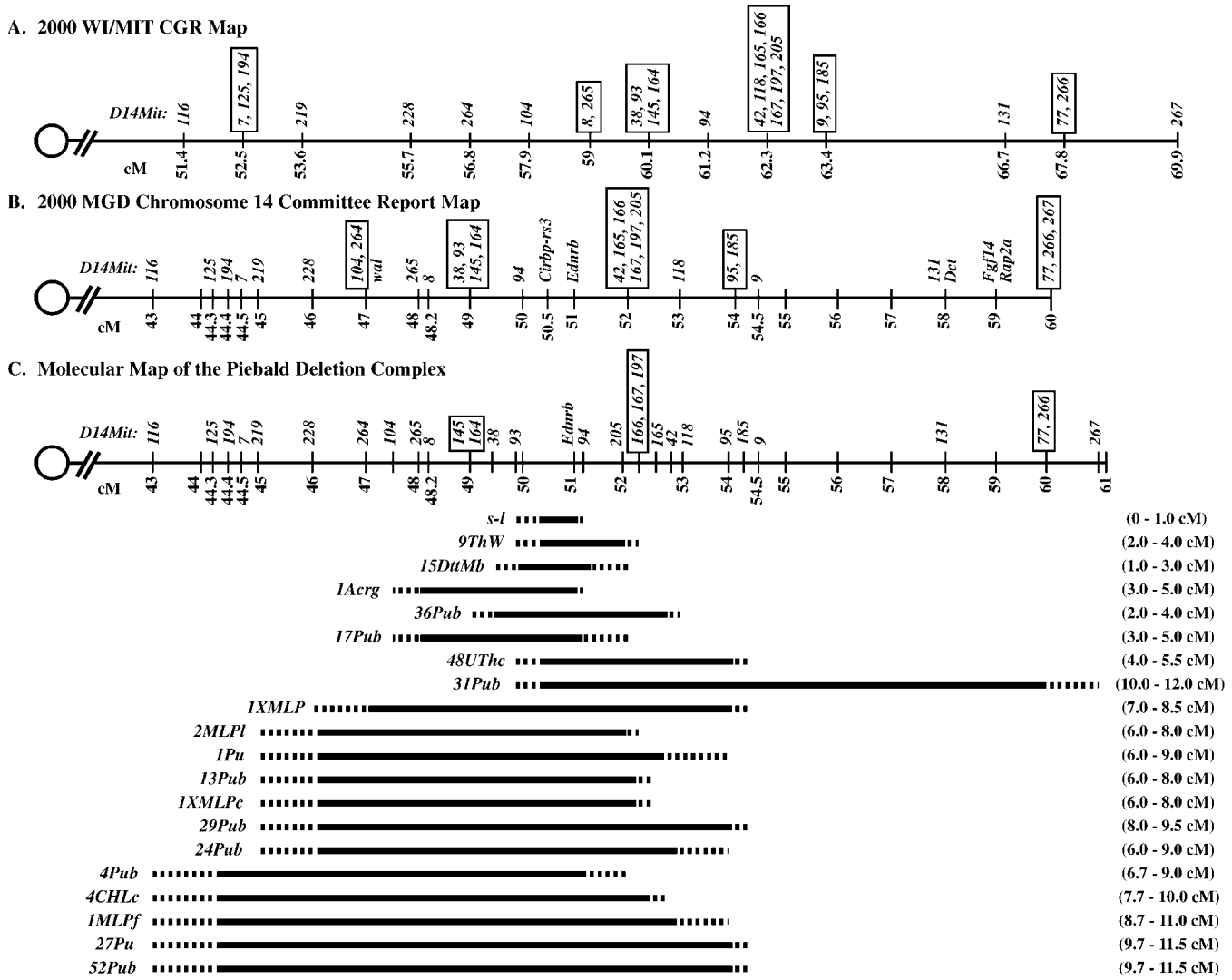

FIGURE 1.—(A–C) Comparative maps of the piebald deletion complex region. The centromere is represented on the left and genetic distance in centimorgans from the centromere is indicated by the numbers just beneath the chromosome for each map. (A) Distribution and genetic position of *D14Mit* markers according to the 2000 WI/MIT CGR map. (B) 2000 Mouse Genome Database Chromosome 14 Committee Report genetic map. The *D14Mit* markers used in the analysis of the deletion alleles are distributed according to their genetic position along the chromosome. A subset of the genes assigned to the region is represented above the chromosome and includes *wal* (waved alopecia), *Cirbp-rs3* (cold-inducible RNA-binding protein, related sequence 3), *Ednrb* (endothelin-B receptor), *Dct* (dopachrome tautomerase), *Fgf14* (fibroblast growth factor 14), and *Rap2a* (RAS-related protein 2a). Genes mapping within functional intervals associated with the phenotypes defined in this study include *Ednrb*, which was previously excluded as a candidate (O'BRIEN *et al.* 1996), and *Cirbp-rs3*, which was positioned between markers *D14Mit94* and *D14Mit205*. In this study *Cirbp-rs3* was not mapped against the deletion panel or further evaluated as a candidate gene. (C) Piebald deletion complex map. This map integrates the data from the WI/MIT CGR and MGD/CCR genetic maps and the molecular marker analysis of the piebald deletions. Genetic positions are based on the MGD/CCR genetic map. The deletion limits are defined by the presence or absence of the *D14Mit* markers that have been concurrently ordered against the deletion panel map. *D14Mit* marker order as determined by the deletion breakpoints was consistent with the distribution of the markers from both the MGD CCR and WI/CGR maps and in a number of instances confirmed or afforded further resolution of marker position. Unresolved markers are grouped within a box. Solid lines depict the confirmed extent of each deletion on the basis of the absence of the *D14Mit* markers. Dashed lines represent the regions containing the deletion breakpoint. The order of the markers *D14Mit: 7, 8, (145, 164), 38, 93, 94, 166 (42, 165), 118*, and *9* and the breakpoints of the *15DttMb, 36Pub, 1Acrg, 17Pub, 24Pub, 4CHLc*, and *4Pub* deletions are as previously reported and have been refined as indicated on the current map (METALLINOS *et al.* 1994; O'BRIEN *et al.* 1996). Deletion allele names are to the left and size ranges in centimorgans are listed to the right.

region; however, in a number of instances several breakpoints localized to a specific interval. Therefore, this collection of deletions offers very high genetic resolution for some regions where several breakpoints are clustered, but not for other regions that contain fewer breakpoints.

The placement of the breakpoints relative to the *D14Mit* SSLP markers identified deletions that could be

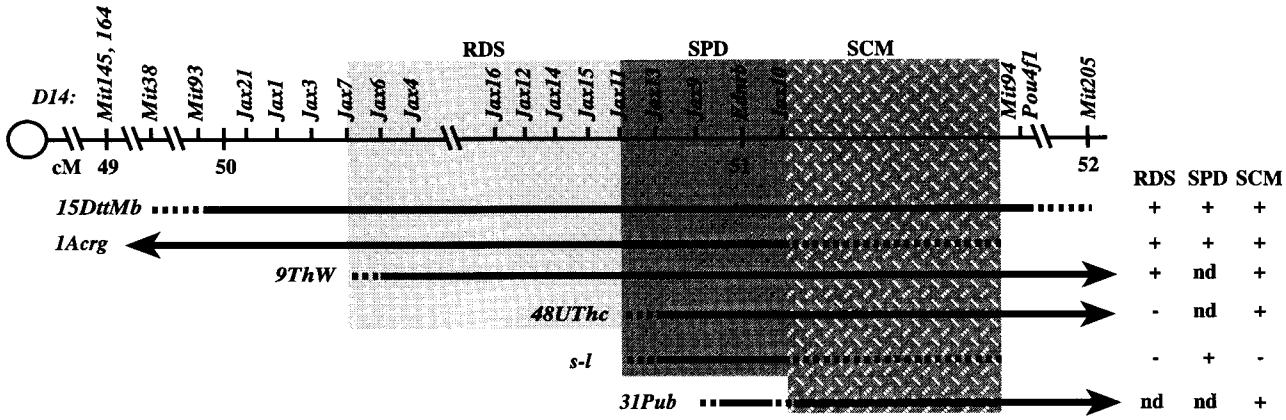

FIGURE 2.—Functional mapping of the *15DttMb*-associated phenotypes. Deletion alleles used in the various complementation crosses are shown below the chromosome. The centromere is on the left and *D14Mit* markers are listed above the chromosome with their distance from the centromere in centimorgans based on the MGD/CCR chromosome 14 genetic map listed below. The *D14Jax* STS markers ordered according to their BAC contig physical map position are listed above the chromosome. The *D14Jax* markers were used to localize the breakpoints of the *1Acrg*, *9ThW*, *48UThc*, *Ednrb*$^{s\text{-}l}$, and *31Pub* deletions. The solid lines represent the confirmed extent of each deletion on the basis of the absence of the molecular markers. The dashed lines depict the regions containing the deletion breakpoint. Associated phenotypes based on the results of the complementation analysis are summarized to the right of each deletion. The critical regions for identifying genes responsible for respiratory distress (light gray), skeletal patterning defects (dark gray and cross-hatched dark gray), and malformation of the dorsal spinal cord (cross-hatched dark gray) are indicated. Assuming an even distribution of the defining proximal breakpoints to partition 1.0 cM into three intervals, the respiratory distress syndrome (RDS) critical region is estimated to be 0.33 cM. The sizes of the skeletal patterning defects (SPD) and spinal cord malformation (SCM) critical regions are based on the YAC/BAC physical map and are estimated to be 800 and 600 kb, respectively. nd, not determined.

used for further functional analysis of specific chromosomal regions. In previous studies, respiratory failure, skeletal patterning, and CNS defects were associated with a 1.1-cM functional interval defined by the *15DttMb* proximal and *1Acrg* distal breakpoints, a region delimited by *D14Mit38* and *D14Mit94*, and containing *D14Mit93*, which is absent in the *15DttMb* deletion chromosome. On the basis of the presence of *D14Mit93*, four deletions (*9ThW*, *48UThc*, *31Pub*, and the spontaneous *Ednrb*$^{s\text{-}l}$ allele) were identified with proximal breakpoints located within the critical interval. To resolve the distribution of these proximal breakpoints we used sequence-tagged site (STS) markers derived from BAC clones that had been assembled into contigs during the construction of a physical map of the region (S. J. WARNER, A. BROWN and T. P. O'BRIEN, unpublished results). The presence or absence of the STS markers was assessed in PCR assays using DNAs from homozygous deletion or compound heterozygous deletion mice; therefore, a polymorphism was not required. The STS content determined for the deletion chromosomes was consistent with the marker arrangement predicted from the physical map. These analyses established the proximal-distal order of the proximal deletion breakpoints in the interval as (1) *9ThW*, (2) *48UThc* and *Ednrb*$^{s\text{-}l}$, which were not resolved using the available markers, and (3) *31Pub* (see Figure 2). The distal breakpoints of the *9ThW*, *48UThc*, and *31Pub* deletions are distal to *D14Mit94* and thus fall outside the critical region, while the distal breakpoints of the *Ednrb*$^{s\text{-}l}$ and *1Acrg* deletions were not resolved and are defined by *D14Mit94* at the distal end of the functional interval. The STS content mapping of the *31Pub* deletion revealed a marker, *D14Jax10*, that appeared to be present and flanked by molecular markers that were absent, suggesting that this could be a noncontiguous deletion.

Previous studies had also identified another functional interval, located at the distal end of the *36Pub* deletion, associated with abnormal skeletal morphogenesis (O'BRIEN *et al.* 1996). The *15DttMb* distal and *36Pub* distal breakpoints define this ~2.0-cM critical region that is delimited by the *D14Mit94* and *D14Mit118* molecular markers. Based on our survey, seven deletions were identified as having distal breakpoints located within this functional interval. To resolve these breakpoints we used all of the six available *D14Mit* SSLP markers that mapped between *D14Mit94* and *D14Mit118* at 52 cM on the MGD/CCR genetic map (Figure 3). For this analysis, polymorphisms and homozygous or compound heterozygous deletion DNAs were used to determine *D14Mit* marker content. The results established the proximal-distal order of the distal deletion breakpoints as (1) *15DttMb*, *4Pub*, and *17Pub* (unresolved), (2) *2MLPl* and *9ThW* (unresolved), (3) *1XMLPc* and *13Pub* (unresolved), (4) *4CHLc*, and finally (5) *36Pub*. Concurrently, the deletions assisted in ordering the *D14Mit* markers, improving the resolution over the current genetic map (see Figures 1 and 3).

Complementation analysis of the *15DttMb*-associated lethality: Mice homozygous for the *15DttMb* deletion

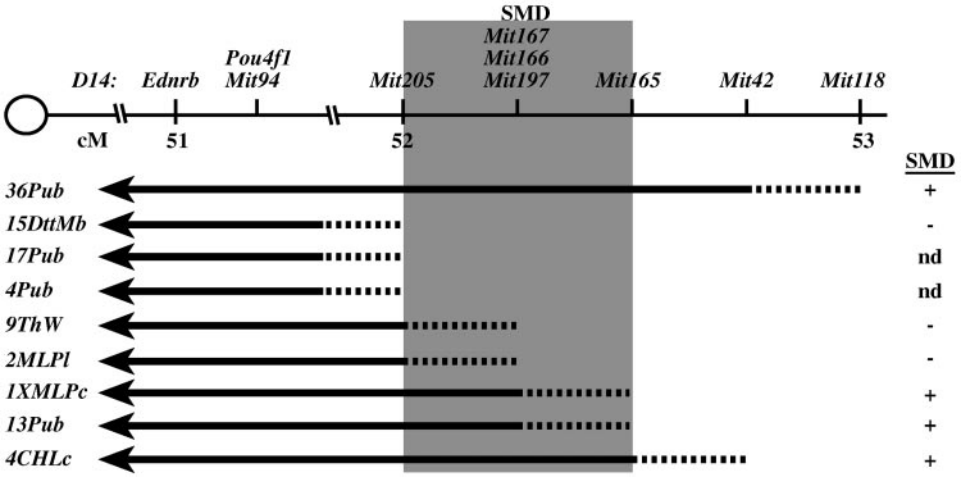

FIGURE 3.—Functional mapping of the *36Pub*-specific skeletal defects. Deletion alleles used in the various complementation crosses are shown below the chromosome. The centromere is on the left and *D14Mit* markers are listed above the chromosome with their distance from the centromere in centimorgans based on the MGD/CCR chromosome 14 genetic map listed below. The panel of *D14Mit* markers mapping at 52 cM was used to localize the distal breakpoints of the deletions shown. The solid lines represent the confirmed extent of each deletion on the basis of the absence of the molecular markers. The dashed lines depict the regions containing the deletion breakpoint. Presence or absence of the *36Pub*-specific skeletal defects based on the complementation studies is summarized to the right of each deletion. The critical region for identifying the gene(s) responsible for the skeletal and cartilage defects (gray) is indicated. Assuming an even distribution of the defining distal breakpoints to partition 1.0 cM into five intervals, the skeletal morphogenesis defects (SMD) critical region is estimated to be 0.20 cM. nd, not determined.

display respiratory distress and die within ~30 min following Caesarian delivery at E18.5. Previous studies determined that the *1Acrg* deletion fails to complement the recessive lethality localizing this functional interval to the proximal portion of the *15DttMb* deletion. In an effort to further define the critical region for identifying the gene(s) responsible for lethality we performed complementation studies using two deletions, *9ThW* and *48UThc*, that provide additional DNA covering the proximal portion of the *15DttMb* deletion (see Figure 2). In our experiments ~75% of the control littermates delivered at E18.5 breathe and are viable beyond 30 min. *15DttMb/9ThW* compound heterozygotes were recovered at E18.5; however, all of these mice presented respiratory distress and died within 30 min following delivery. In contrast, 80% of the E18.5 *15DttMb/48UThc* compound heterozygotes breathed and were viable (Table 3).

In parallel to the crosses to determine whether the *9ThW* and *48UThc* chromosomes could rescue respiratory failure we designed crosses using these deletions that had the potential to produce viable juvenile mice as evidence for complementation. The *15DttMb* allele was not suitable for these experiments since the *Pou4f1* gene (formerly *Brn 3.0*) maps to the distal portion of this deletion. *Pou4f1* loss-of-function mutants die within 24 hr of birth and present several defects related to abnormal CNS development including defective swallowing, presumably owing to the mismigration of compact formation neurons that normally populate the nucleus ambiguus and innervate the esophagus (MCEVILLY *et al.* 1996; XIANG *et al.* 1996). On the basis of the position of their distal breakpoints, the *9ThW* and *48UThc* deletions also remove the *Pou4f1* gene. Therefore, *15DttMb/9ThW* and *15DttMb/48UThc* compound heterozgotes would be expected to present the *Pou4f1* mutant phenotype and die within a day of birth. Instead, for these studies we used the *1Acrg* deletion. This deletion fails to rescue the respiratory failure; however, this chromosome does not remove the *Pou4f1* gene and supports its normal expression during development (I. C. WELSH and T. P. O'BRIEN, unpublished observations). *1Acrg/48UThc* compound heterozygotes were viable and presented the *Ednrb* mutant phenotype of an almost completely white coat and lethality resulting from megacolon at ~3–4 weeks of age (Table 3). In contrast, a white mouse was never observed in the progeny from crosses between *1Acrg* and *9ThW* heterozygotes and five dead newborn pups were recovered that genotyped as *1Acrg/9ThW* compound heterozygotes. Together these studies demonstrate that the *15DttMb* lethality is rescued by the *48UThc* deletion but not the *9ThW* deletion. This localizes the gene(s) responsible for respiratory distress to a region defined by the *9ThW* and *48UThc* proximal breakpoints (Figure 2).

Complementation analysis of the *15DttMb*-associated spinal cord malformation: The *15DttMb* mutants also displayed CNS abnormalities including an alteration in the architecture of the dorsal spinal cord. The fully penetrant malformation involved a dorsolateral extension of cells in the dorsal horns into the region normally occupied by the overlying nerve tracts and ectopic cells scattered throughout the dorsal funiculus (Figure 4). Altered cellular distribution and differentiation were evident along the entire rostrocaudal length of the spinal cord and appeared coincident with the formation of dorsal neuronal cell types arising between E12.5 and E14.5. Previous complementation studies had defined an interval contained by the *15DttMb* proximal and the *1Acrg* distal breakpoints associated with the phenotype

TABLE 3

Incidence of *15DttMb*-associated respiratory distress and lethality

	No. of litters	No. of progeny	Genotype	Genotype	Genotype
Respiratory distress					
			+/+	*15DttMb* or *48UThc*/+	*15DttMb*/*48UThc*[a]
15DttMb × *48UThc*	2	15	5 (33)	5 (33)	5 (33)
			+/+	*15DttMb* or *9ThW*/+	*15DttMb*/*9ThW*[a]
15DttMb × *9ThW*	3	12	2 (16)	6 (50)	4 (33)
Lethality					
			+/+	*1Acrg* or *9ThW*/+	*1Acrg*/*9ThW*[b]
1Acrg × *9ThW*	6	31	14 (45)	12 (39)	5 (16)
			+/+	*1Acrg* or *48UThc*/+	*1Acrg*/*48UThc*[c]
1Acrg × *48UThc*	3	21	8 (38)	9 (43)	4 (19)

Values in parentheses are percentages.

[a] Pups breathing successfully 30 min following Caesarian delivery were scored as viable. Four of the five *15DttMb*/*48UThc* pups were viable. In contrast, none of the *15DttMb*/*9ThW* pups were viable.

[b] Progeny genotyping as *1Acrg*/*9ThW* were recovered as dead pups shortly after delivery.

[c] One of the *1Acrg*/*48UThc* mice died shortly after birth and three survived to present the *Ednrb* loss-of-function phenotype of an almost completely white coat and juvenile lethality owing to megacolon.

(O'Brien *et al.* 1996). The mapping of additional deletion limits again identified a group of alleles useful for studies to further localize the gene(s) underlying abnormal *15DttMb* spinal cord development.

In this study the spinal cord malformation was evident in transverse sections of E14.5 *15DttMb* homozygotes ($n = 2$) and *15DttMb*/*1Acrg* compound heterozygotes ($n = 2$) that are predominantly on a C57BL/6J genetic background (N6). The spinal cord dysmorphology was directly comparable to that described using the mouse stocks on the mixed genetic background originally used to characterize the phenotype (O'Brien *et al.* 1996). A series of complementation crosses revealed that the *15DttMb*/*9ThW* ($n = 3$), *15DttMb*/*48UThc* ($n = 3$), and *15DttMb*/*31Pub* ($n = 3$) compound heterozygotes all displayed spinal cord abnormalities at E14.5. In contrast, the spinal cord morphology of E14.5 *Ednrb*$^{s\text{-}l}$ deletion homozygotes ($n = 3$) was normal (Figure 4 and data not shown). On the basis of molecular mapping of these deletions the *31Pub* chromosome extends to provide the most DNA covering the proximal portion of the previously defined critical region, yet it fails to comple-

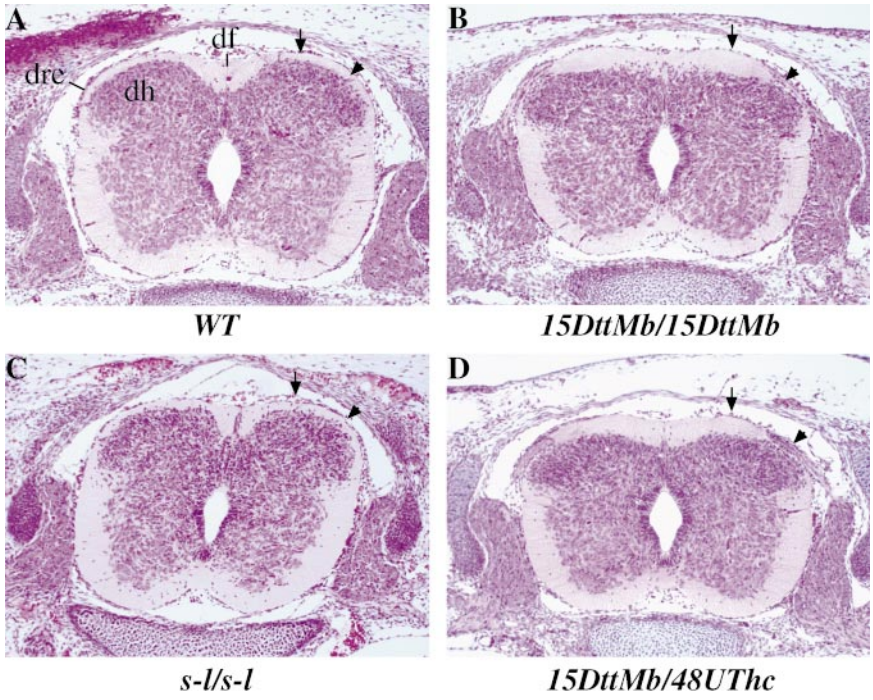

Figure 4.—Complementation analysis of the *15DttMb* dorsal spinal cord malformation. (A and B) Thoracic level transverse sections through the spinal cord of (A) an E14.5 wild-type littermate and (B) E14.5 *15DttMb* mutant demonstrate the morphological alterations that include a dorsolateral extension of the dorsal horns (arrowhead), thickening of the overlying white matter (arrow), and the shallow appearance of the dorsal funiculus. (C and D) Thoracic level transverse sections through the spinal cord of (C) an E14.5 *Ednrb*$^{s\text{-}l}$ mutant showing normal morphology and (D) an E14.5 *15DttMb*/*48UThc* compound heterozygous mutant demonstrating the disorganization of the developing spinal cord as seen in the *15DttMb* mutant. df, dorsal funiculus; dh, dorsal horn; dre, dorsal root entrance zone.

TABLE 4

Incidence of *15DttMb*-associated skeletal defects

	Genotype			
	s/s[a]	*s-l/s*[a]	*s-l/s-l*[a]	*15DttMb/15DttMb*[b]
Total	8	27	17	41
Sternal defects	0	2 (7)	3 (18)	12 (29)
Eight vertebrosternal ribs	0	0	0	4 (10)
Ribs on L1	0	0	0	17 (41)
Posterior shift of sacrum	1 (12.5)	16 (59)	17 (100)	41 (100)

Values in parentheses are percentages.
[a] Progeny from intercross mating of SSL/Le *s-l/s* × *s-l/s* or *s-l/s* × *s-l/s-l* mice.
[b] Data from previous analysis of *15DttMb* skeletal patterning defects (O'Brien *et al.* 1996).

ment the phenotype. All of the deletions used in these crosses have distal breakpoints that extend beyond the *Ednrb*$^{s\text{-}l}$ and *1Acrg* distal breakpoints, which have not been resolved by the marker analysis. This suggests that the *Ednrb*$^{s\text{-}1}$ deletion rescues the *15DttMb* spinal cord phenotype by providing DNA covering a portion of the critical region distal to the *Ednrb* gene that is absent in the *1Acrg* deletion (Figure 2).

Complementation analysis of *15DttMb*-associated skeletal defects: In our initial characterization of the *15DttMb* mutants we described anterior homeotic transformations of vertebral identity comparable to those reported for several mutations that result in the loss of *Hox* gene function. In contrast to the respiratory failure and CNS defects, the *15DttMb* skeletal phenotype displayed variable penetrance and expressivity potentially resulting from the heterogeneous genetic background of the deletion stock mice (O'Brien *et al.* 1996). In an effort to further define the functional interval associated with the vertebral transformations we analyzed the skeletons of *Ednrb*$^{s\text{-}1}$ deletion mutants derived from crosses using the SSL/Le inbred stock of *Ednrb*^{s}/*Ednrb*$^{s\text{-}l}$ compound heterozygous mice (Table 4). The variably penetrant anterior transformations resulting in eight vertebrosternal ribs rather than the normal seven, or an extra set of ribs on the first lumbar vertebra (L1) as seen in the *15DttMb* mutants, were not observed in the *Ednrb*$^{s\text{-}1}$ homozygotes. However, in all of the *Ednrb*$^{s\text{-}l}$ homozygotes the first sacral vertebra adopted a more anterior lumbar vertebral identity, shifting the position of the sacrum one segment more posterior than observed in the *Ednrb*^{s} control mice (Figure 5). A posterior shift in the lumbosacral transition compared to control littermates is identical to the sacral phenotype observed in the *15DttMb* homozygous skeletons. In addition, some of the *Ednrb*$^{s\text{-}l}$ homozygotes and heterozygotes exhibited malformed sternebrae owing to rib misalignments as seen in the *15DttMb* homozygous skeletons. Interestingly, a significant number of *Ednrb*$^{s\text{-}l}$ deletion heterozygous mice also displayed a posterior shift in sacral position (Table 4). Modifying effects exposed by the inbred SSL/Le genetic background potentially account for the previously unseen dosage sensitivity of the sacral phenotype.

Complementation analysis of *36Pub*-associated skeletal defects: The ~3.0-cM *36Pub* deletion encompasses the ~1.5-cM *15DttMb* deletion. The *36Pub* mutants exhibit the *15DttMb* lethality and CNS phenotype. Distinct from the *15DttMb* skeletal defects, malformations of the axial and cranial skeleton, including fused ribs, dysmorphology and fusion of cervical vertebrae, abnormal formation of bones in the skull, and cleft palate have been described in the *36Pub* mutants. These *36Pub*-specific skeletal defects have been localized to the distal end

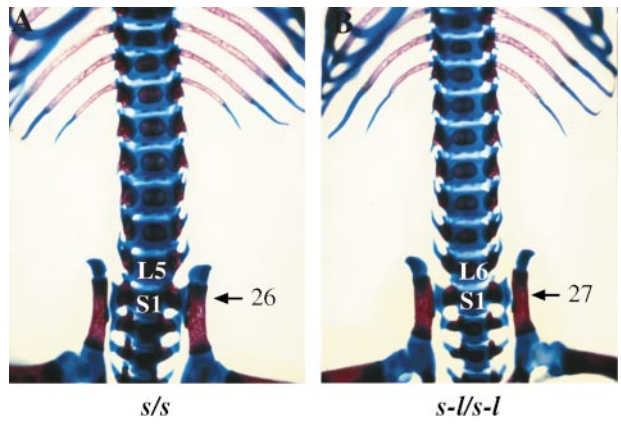

Figure 5.—Altered position of the lumbosacral transition in *Ednrb*$^{s\text{-}l}$ homozygous mice. (A) E18.5 *Ednrb*^{s} homozygous control showing five lumbar vertabrae (L5) and a first sacral vertebra (S1) corresponding to the 26th vertebral segment. This normal variation that is typically observed in ~10% of the mice from several inbred strains was seen in 87.5% of the mice genotyping as *Ednrb*^{s}/*Ednrb*^{s} (Grüneberg 1952; Kessel and Gruss 1991; Le Mouellic *et al.* 1992). (B) E18.5 *Ednrb*$^{s\text{-}l}$ mutant showing six lumbar vertebrae (L6) and a first sacral vertebra (S1) corresponding to the 27th vertebral segment. This posterior shift in sacral position relative to the *Ednrb*^{s} control was evident in 100% of the mutants (see Table 4).

of this deletion between the *15DttMb* and *36Pub* distal breakpoints (O'Brien *et al.* 1996). In addition to the variably penetrant skeletal defects, highly penetrant malformations involving thickened and fused cartilaginous elements of the trachea, neural arches of the lumbar and sacral vertebrae, digits on both the fore- and hindlimbs, and structures in the skull have been observed in *36Pub* homozygotes. Cartilage defects are also seen at a reduced penetrance in the *36Pub* heterozygotes.

In an effort to further define the critical region associated with the *36Pub* skeletal defects we examined skeletons representing several allelic combinations using the deletions identified as having distal breakpoints positioned within the functional interval (Figure 6). *36Pub*-specific defects were not observed in *36Pub/ 9ThW* and *36Pub/ 2MLPl* compound heterozygous skeletons (Table 5). Therefore, although the *9ThW* and *2MLPl* distal breakpoints extend beyond the *15DttMb* distal breakpoint, these deletions do not remove the gene(s) responsible for the *36Pub*-specific skeletal defects. In contrast, *36Pub/ 1XMLPc*, *36Pub/ 13Pub*, and *36Pub/ 4CHLc* mutants presented the *36Pub*-associated skeletal phenotype (Table 5). These deletions failed to complement the *36Pub*-specific skeletal defects, which is consistent with the placement of their distal breakpoints beyond the distal limits of the *9ThW* or *2MLPl* deletions. The molecular marker analysis has placed the *4CHLc* distal breakpoint beyond the *1XMLPc* and *13Pub* distal breakpoints, localizing the gene(s) important for skeletal morphogenesis to a functional interval defined by the *9ThW* (or *2MLPl*) distal and *1XMLPc* (or *13Pub*) distal breakpoints (Figure 3). The development of additional markers permitting resolution of the *9ThW* and *2MLPl*, and the *1XMLPc* and *13Pub*, distal breakpoints will further refine the critical region. Interestingly, several allelic combinations, *36Pub/ 9ThW*, *36Pub/ 2MLPl*, *1XMLPc/+*, *13Pub/+*, and *4CHLc/+*, did not present the *36Pub* haploinsufficient cartilage defects at a frequency comparable to that seen in the original analysis of the *36Pub*-specific skeletal phenotype (see Table 5). However, the complementation crosses were performed using mice on a predominantly C57BL/6J genetic background and although the *36Pub* recessive skeletal defects were highly penetrant on a C57BL/6J genetic background (N6), the haploinsufficient cartilage defects on the C57BL/6J genetic background were reduced compared to those observed in the *36Pub* heterozygous skeletons from the deletion stock mice used in previous studies.

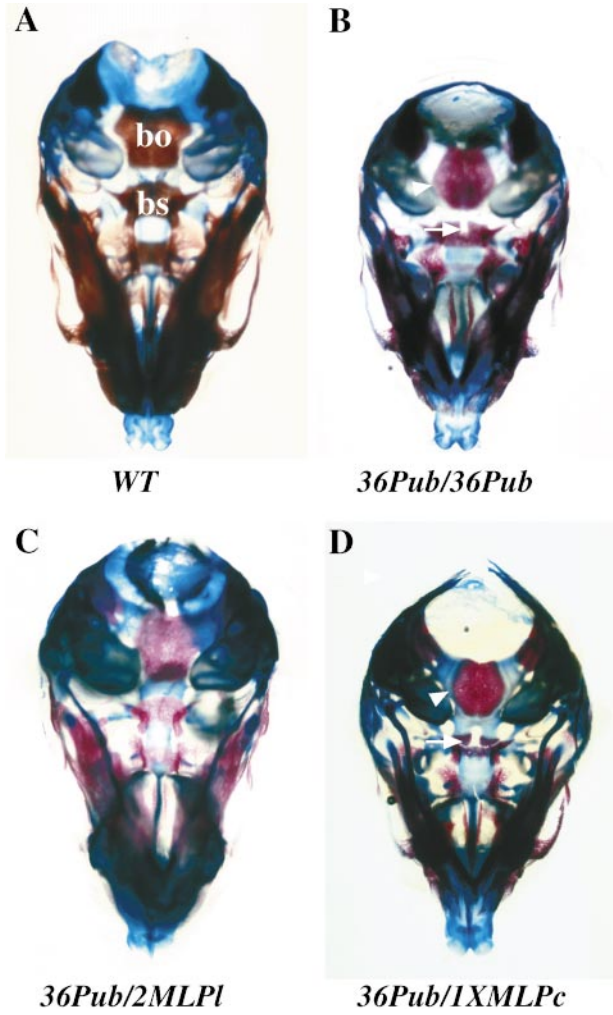

Figure 6.—Complementation analysis of the *36Pub* skeletal defects. (A and B) Ventral views of the skulls from (A) an E18.5 wild-type littermate and (B) an E18.5 *36Pub* mutant demonstrating the rounded appearance of the basioccipital bone (arrowhead) and the incomplete formation of the basisphenoid bone showing a persistence of the hypophyseal foramen (arrow). (C and D) Ventral views of the skulls from (C) an E18.5 *36Pub/ 2MLPl* compound heterozygous mutant showing normal cranial skeletal morphology and (D) an E18.5 *36Pub/ 1XMLPc* compound heterozygous mutant demonstrating *36Pub*-specific cranial skeletal defects. Also note the thickened cartilage surrounding the basioccipital bone. bo, basioccipital bone; bs, basisphenoid bone.

DISCUSSION

The deletion complexes generated during the SLT have provided important resources for studying genome structure and function. In this study we have characterized 20 alleles of the piebald deletion complex centered around the *Ednrb* locus on distal mouse chromosome 14. The *D14Mit* SSLP marker-based and STS-based molecular analysis of these deficiencies has ordered the position of the deletion breakpoints and provided a framework for integrating genetic, physical, and functional information for this chromosomal region.

The piebald deletion complex encompasses a 15.7- to 18-cM interval delimited by the *D14Mit* markers positioned on the MGD/CCR genetic map. The extent of the deletion complex is consistent with the recovery of viable heterozygous mice cytogenetically defined as

TABLE 5

Incidence of *36Pub*-associated skeletal defects

	Genotype												
	+/+	*36Pub/9ThW*	*36Pub/2MLPl*	*36Pub/1XMLPc*	*1XMLPc/+*	*36Pub/13Pub*	*13Pub/+*	*36Pub/4CHLc*	*4CHLc/+*	*36Pub/36Pub*[b]		36Pub/+[b]	
Total	43	5	5	5	10	3	2	4	7	5		44	
Cleft palate[a]	0/34	0/4	0/5	1/5 (20)	0/6	1/3 (33)	0	3/3 (100)	0/4	4/5 (80)	(74)	0/32	
Basisphenoid incomplete	0	0	0	5 (100)	0	3 (100)	0	2 (50)	0	5 (100)	(64)	0	
Basioccipital rounded	0	0	0	5 (100)	0	3 (100)	0	3 (75)	0	5 (100)	(88)	3 (7.5)	
Axis (C2) malformations	0	0	0	5 (100)	0	3 (100)	0	3 (75)	0	5 (100)	(51)	3 (7.5)	
Fused ribs													
6 and 7	0	0	0	3 (60)	0	3 (100)	0	2 (50)	0	3 (60)	(19)	0	
Cartilage malformations													
Hyoid	0	0	0	5 (100)	0	3/3 (100)	2 (100)	3 (75)	1 (14)	5 (100)	(97)	3 (7.5)	(31)
Larynx	0	0	0	4 (80)	0	3/3 (100)	0	3 (75)	0	5 (100)	(97)	2 (5)	(8)
Trachea	0	0	0	4 (80)	0	3/3 (100)	0	2 (50)	0	3 (60)	(95)	0	(28)
Neural arches	0	0	0	5 (100)	0	3/3 (100)	0	3 (75)	2 (29)	5 (100)	(97)	1 (2.5)	(6)
Digits	0	0	0	5 (100)	0	3/3 (100)	0	3 (75)	0	5 (100)	(97)	1 (2.5)	(0)

Values in parentheses are percentages.

[a] Subset of mice permitting a definitive assessment of palatal development are represented.

[b] Data (percentages only; only cartilage malformations are listed for *36Pub/+* mice) from the previous analysis of *36Pub* skeletal defects are provided to the right for comparison (O'Brien *et al.* 1996).

having lost 26–30% (14E1–E4) of the distal region of chromosome 14 (Cattanach *et al.* 1993). The proximal boundary of the complex extends 8 cM from the *Ednrb* focal point. This proximal limit is shared by a group of five large deletions estimated to range in size from 6.7 to 11.5 cM. The distal limit of the complex extends 10 cM from the *Ednrb* focal point. In this study a single deletion, *31Pub*, defines the distal end of the complex. However, the Mammalian Genetics Unit, Harwell, United Kingdom, reports several piebald deletions that encompass the *Dct*^{slt} locus (slatey) that maps with the marker *D14Mit131* used in the analysis of *31Pub*, suggesting that these deletions have comparable distal limits (http://www.mgu.har.mrc.ac.uk/). Interestingly, the molecular mapping suggested a discontinuity in the *31Pub* deletion. Therefore, although our analysis indicates that several distal markers are uniquely absent in this deletion, it potentially represents a more complex chromosomal rearrangement. Molecular evidence supporting the occurrence of noncontiguous deletions has also been reported in the analysis of the SLT-derived albino, brown, dilute-short ear, and pink-eyed dilution deletion complexes (Russell 1971; Sharan *et al.* 1991; Bell *et al.* 1995; Johnson *et al.* 1995; Rikke *et al.* 1997). Although a significantly higher density of markers will be required to fully address this issue, the results of our analysis, along with the other SLT deletion complex studies using the resolution afforded thus far, suggest that noncontiguous deletions are uncommon.

The molecular marker analysis positioned each deletion breakpoint relative to a defined region on the current MGD/CCR genetic map. This analysis did not identify deletions in addition to the previously characterized *17Pub* with breakpoints useful for further refining the ~0.8-cM functional interval associated with perturbed mesoderm development leading to midgestational lethality of the *1Acrg* mutant embryo (Welsh and O'Brien 2000). However, a 1.4-Mb BAC contig has been assembled over this critical region and is being used for the identification of candidate genes (Kurihara *et al.* 2000). Several of the deletion breakpoints were positioned within the previously characterized functional intervals associated with genes that are essential for newborn survival and normal skeletal and CNS development. In these regions, all of the available *D14Mit* SSLP markers or STS markers derived from BAC ends were used to construct higher resolution maps (Figures 2 and 3). The ordering of the breakpoints within these specific intervals permitted the selection of the deletion alleles used in this study for functional mapping.

A complex set of phenotypes that included respiratory failure at birth, abnormal spinal cord development, and skeletal patterning defects was previously mapped within a 0.5- to 1.1-cM interval at the proximal end of the *15DttMb* deletion (O'Brien *et al.* 1996). Four deletions identified as having breakpoints positioned within this critical interval were used for complementation analysis. On the basis of the characterization of various deletion homozygous and compound heterozygous mice, the phenotypes were separated genetically and localized to defined chromosomal intervals (Figure 2). The *48UThc* deletion was able to rescue the *15DttMb* neonatal lethality localizing the gene(s) associated with respiratory distress to an estimated 0.33-cM region at the proximal end of the noncomplementing *9ThW* deletion. *Ednrb*$^{s\text{-}l}$ homozygous mice exhibited a posterior shift in the position of the sacrum and sternal defects comparable to the *15DttMb* mutants. This focuses the search for candidate genes involved in skeletal patterning to an estimated 800-kb region covered by a yeast artificial chromosome (YAC)/BAC physical map that spans the *Ednrb*$^{s\text{-}l}$ deletion (S. J. Warner, H. Chen, D. L. Metallinos, S. M. Tilghman and T. P. O'Brien, unpublished observations). Finally, *Ednrb*$^{s\text{-}l}$ mutants did not exhibit a spinal cord malformation, whereas the *48UThc* and *31Pub* deletions failed to rescue the spinal cord defect despite having proximal breakpoints that map with or extend beyond the *Ednrb*$^{s\text{-}l}$ proximal breakpoint, respectively. On the basis of these results we favor the interpretation that the spinal cord phenotype is associated with a region distal to the *Ednrb* locus that is present in the *Ednrb*$^{s\text{-}l}$ chromosome and is commonly removed by the noncomplementing *1Acrg*, *9ThW*, *48UThc*, and *31Pub* deletions. This functional interval, defined by the *Ednrb*$^{s\text{-}l}$ and *1Acrg* distal breakpoints, is estimated to be <600 kb on the basis of the YAC/BAC physical map that covers the region. Identification of the molecular basis of the phenotypes will provide insight into whether separate genes are responsible for the *15DttMb* developmental defects as suggested by the results of the complementation analysis.

Defects in skeletal and cartilage morphogenesis had been previously localized to a 1.1-cM interval at the distal end of the *36Pub* deletion (O'Brien *et al.* 1996). Five deletions with distal breakpoints positioned within this critical region were selected for functional mapping. Two of these deletions, *9ThW* and *2MLPl*, were able to complement, whereas the more distally extending *1XMLPc* and *13Pub* and the most distally extending *4CHLc* deletions failed to rescue the *36Pub*-specific skeletal defects. The noncomplementing allelic combinations presented the full range of *36Pub*-specific defects including cleft palate, cranial and axial skeletal, and cartilage malformations, suggesting the possibility that the skeletal phenotype represents the loss of a single gene. Efforts to determine the molecular basis of the phenotype will focus on the identification of candidate genes located within an estimated 0.20-cM functional interval defined by the *9ThW* (or *2MLPl*) and *1XMLPc* (or *13Pub*) distal breakpoints (Figure 3).

The recent advances for engineering defined chromosomal deficiencies using *Cre/LoxP* or using a positive/negative selectable marker with radiation to generate deletion complexes in germline-competent

embryonic stem cells allow the approaches used in SLT deletion complex studies to be directed toward any region of the genome (Ramírez-Solis *et al.* 1995; You *et al.* 1997; Thomas *et al.* 1998). A deletion complex represents a valuable tool for assembling comprehensive maps of defined chromosomal regions. Deletion panels enrich the use of backcross and radiation hybrid panels and YAC/BAC contig information for determining marker order and establishing genetic and physical distance relationships. Importantly, deletion complexes also represent a resource for dissecting the functional content of a specific genomic region (Justice *et al.* 1997; Schimenti and Bucan 1998). Our efforts have focused on using the piebald deletion complex to uncover genes that are important for development. In addition to characterizing those deletions used in the functional mapping studies we have identified several large deletions, such as *52Pub* and *31Pub*, that in combination could remove as many as 785–900 genes assuming ~80,000 genes per ~1600-cM haploid genome (15.7–18 cM/1600 cM × 80,000).

In an effort to identify those genes that are essential for normal development we have initiated a regionally directed ENU mutagenesis screen. The screen takes advantage of the piebald coat color phenotype to mark the offspring that potentially carry an ENU-induced point mutation opposite a large piebald deletion. An ENU-induced mutation that disrupts a gene required for development results in the reduction or loss of the spotted class of mice among the test cross progeny. This strategy has been used to identify several essential loci that map within the albino deletion complex and has generated an allelic series of mutations for the homeotic regulatory gene *eed* (Rinchik *et al.* 1990; Schumacher *et al.* 1996; Rinchik and Carpenter 1999). The recovery of ENU-induced mutations will be valuable for evaluating candidate genes for the lethal phenotypes already identified in the piebald region. The screen also provides the opportunity to uncover a locus whose function was masked by an earlier-acting essential gene within the deletion. Following isolation, an ENU-induced mutation can be readily mapped to a specific interval in complementation crosses using the piebald deletions characterized in this study. The analysis and application of the piebald deletions have advanced efforts to isolate genes critical for survival after birth, gastrulation, spinal cord development, and skeletal patterning and morphogenesis. This study has also established this resource for future efforts to generate a functional map of the distal region of mouse chromosome 14.

We thank Stephen Warner and Aaron Brown for assisting with the development the BAC-derived STS markers, and Lisa Ford and Gretchen Kaiser for assistance in maintaining the mouse colonies. We also thank Drs. Greg Cox, John Schimenti, Shirley Tilghman, and Ian Welsh for valuable discussions and critically reading the manuscript. This work was supported by National Institutes of Health grant HD36434 and the shared service facilities of The Jackson Laboratory Cancer Center (CORE grant CA34196).

LITERATURE CITED

Bell, J. A., E. M. Rinchik, S. Raymond, R. Suffolk and I. J. Jackson, 1995 A high-resolution map of the brown (*b, Tyrp1*) deletion complex of mouse chromosome 4. Mamm. Genome **6:** 389–395.

Cattanach, B. M., M. D. Burtenshaw, C. Rasberry and E. P. Evans, 1993 Large deletions and other gross forms of chromosome imbalance compatible with viability and fertility in the mouse. Nat. Genet. **3:** 56–61.

Davis, A. P., and M. J. Justice, 1998 An Oak Ridge legacy: the specific locus test and its role in mouse mutagenesis. Genetics **148:** 7–12.

Dietrich, W. F., J. Miller, R. Steen, M. A. Merchant, D. Damron-Boles *et al.*, 1996 A comprehensive genetic map of the mouse genome. Nature **380:** 149–152.

Grüneberg, H., 1952 *The Genetics of the Mouse.* Nijhoff, The Hague.

Holdener-Kenny, B., S. K. Sharan and T. Magnuson, 1992 Mouse albino-deletions: from genetics to genes in development. Bioessays **14:** 831–839.

Hosoda, K., R. E. Hammer, J. A. Richardson, A. G. Baynash, J. C. Cheung *et al.*, 1994 Targeted and natural (piebald-lethal) mutations of endothelin-B receptor gene produce megacolon associated with spotted coat color in mice. Cell **79:** 1267–1276.

Johnson, D. K., L. J. Stubbs, C. T. Culiat, C. S. Montgomery, L. B. Russell *et al.*, 1995 Molecular analysis of 36 mutations at the mouse pink-eyed dilution (*p*) locus. Genetics **141:** 1563–1571.

Justice, M. J., B. Zheng, R. P. Woychik and A. Bradley, 1997 Using targeted large deletions and high-efficiency N-Ethyl-N-nitrosourea mutagenesis for functional analyses of the mammalian genome. Methods **13:** 423–436.

Kessel, M., and P. Gruss, 1991 Homeotic transformations of murine vertebrae and concomitant alteration of *Hox* codes induced by retinoic acid. Cell **67:** 89–104.

Kurihara, L. J., E. Semenova, J. M. Levorse and S. M. Tilghman, 2000 Expression and functional analysis of *Uch-L3* during mouse development. Mol. Cell. Biol. **20:** 2498–2504.

Lane, P. W., 1966 Association of megacolon with two recessive spotting genes in the mouse. J. Hered. **57:** 29–31.

Le Mouellic, H., Y. Lallemand and P. Brulet, 1992 Homeosis in the mouse induced by a null mutation in the *Hox–3.1* gene. Cell **69:** 251–264.

McEvilly, R. J., L. Erkman, L. Lou, P. E. Sawchenko, A. F. Ryan *et al.*, 1996 Requirement for *Brn-3.0* in differentiation and survival of sensory and motor neurons. Nature **384:** 574–577.

Metallinos, D. L., 1994 Molecular and genetic characterization of the piebald locus in mice. Ph.D. thesis, Princeton University, Princeton, NJ.

Metallinos, D. L., A. J. Oppenheimer, E. M. Rinchik, L. B. Russell, W. Dietrich *et al.*, 1994 Fine structure mapping and deletion analysis of the murine piebald locus. Genetics **136:** 217–223.

Niswander, L., D. Yee, E. M. Rinchik, L. B. Russell and T. Magnuson, 1989 The albino-deletion complex in the mouse defines genes necessary for development of embryonic and extraembryonic ectoderm. Development **105:** 175–182.

O'Brien, T. P., D. L. Metallinos, H. Chen, M. K. Shin and S. M. Tilghman, 1996 Complementation mapping of skeletal and central nervous system abnormalities in mice of the piebald deletion complex. Genetics **143:** 447–461.

Pavan, W. J., and S. M. Tilghman, 1994 Piebald lethal (*s-l*) acts early to disrupt the development of neural crest-derived melanocytes. Proc. Natl. Acad. Sci. USA **91:** 7159–7163.

Ramírez-Solis, R., P. Liu and A. Bradley, 1995 Chromosome engineering in mice. Nature **378:** 720–724.

Rikke, B. A., D. K. Johnson and T. E. Johnson, 1997 Murine albino-deletion complex: high-resolution microsatellite map and genetically anchored YAC framework map. Genetics **147:** 787–799.

Rinchik, E. M., and D. A. Carpenter, 1999 N-ethyl-N-nitrosourea mutagenesis of a 6- to 11-cM subregion of the *Fah-Hbb* interval of mouse chromosome 7: completed testing of 4557 gametes and deletion mapping and complementation analysis of 31 mutations. Genetics **152:** 373–383.

Rinchik, E. M., and L. B. Russell, 1990 Germ-line deletion mutations in the mouse: tools for intensive functional and physical mapping of regions of the mammalian genome, pp. 121–158 in *Genome Analysis, Vol. 1: Genetic and Physical Mapping.* Cold Spring Harbor Laboratory Press, Cold Spring Harbor, NY.

Rinchik, E. M., D. A. Carpenter and P. B. Selby, 1990 A strategy for fine-structure functional analysis of a 6- to 11-centimorgan region of mouse chromosome 7 by high-efficiency mutagenesis. Proc. Natl. Acad. Sci. USA **87:** 896–900.

Russell, L. B., 1971 Definition of functional units in a small chromosomal segment of the mouse and its use in interpreting the nature of radiation-induced mutations. Mutat. Res. **11:** 107–123.

Russell, L. B., C. S. Montgomery and G. D. Raymer, 1982 Analysis of the albino-locus region of the mouse: IV. Characterization of 34 deficiencies. Genetics **100:** 427–453.

Russell, W. L., 1951 X-ray induced mutations in mice. Cold Spring Harbor Symp. Quant. Biol. **16:** 327–336.

Schimenti, J., and M. Bucan, 1998 Functional genomics in the mouse: phenotype-based mutagenesis screens. Genome Res. **8:** 698–710.

Schumacher, A., C. Faust and T. Magnuson, 1996 Positional cloning of a global regulator of anterior-posterior patterning in mice. Nature **383:** 250–253.

Sharan, S. K., B. Holdener-Kenny, S. Ruppert, A. Schedl, G. Kelsey *et al.*, 1991 The albino deletion complex of the mouse: molecular mapping of deletion breakpoints that define regions necessary for development of the embryonic and extraembryonic ectoderm. Genetics **129:** 825–832.

Shin, M. K., L. B. Russell and S. M. Tilghman, 1997 Molecular characterization of four induced alleles at the *Ednrb* locus. Proc. Natl. Acad. Sci. USA **94:** 13105–13110.

Shin, M. K., J. M. Levorse, R. S. Ingram and S. M. Tilghman, 1999 The temporal requirement for endothelin receptor-B signalling during neural crest development. Nature **402:** 496–501.

Thomas, J. W., C. Lamantia and T. Magnuson, 1998 X-ray-induced mutations in mouse embryonic stem cells. Proc. Natl. Acad. Sci. USA **95:** 1114–1119.

Welsh, I. C., and T. P. O'Brien, 2000 Loss of late primitive streak mesoderm and interruption of left-right morphogenesis in the *1Acrg mutant mouse. Dev. Biol.* **225:** 151–168.

Xiang, M., L. Gan, L. Zhou, W. H. Klein and J. Nathans, 1996 Targeted deletion of the mouse POU domain gene *Brn-3a* causes selective loss of neurons in the brainstem and trigeminal ganglion, uncoordinated limb movement, and impaired suckling. Proc. Natl. Acad. Sci. USA **93:** 11950–11955.

You, Y., R. Bergstrom, M. Klemm, B. Lederman, H. Nelson *et al.*, 1997 Chromosomal deletion complexes in mice by radiation of embryonic stem cells. Nat. Genet. **15:** 285–288.

Communicating editor: N. A. Jenkins